

# Differentiating the Black-Box: Optimization with Local Generative Surrogates

Sergey Shirobokov<sup>\*1</sup> Vladislav Belavin<sup>\*2</sup> Michael Kagan<sup>3</sup> Andrey Ustyuzhanin<sup>2</sup> Atılım Güneş Baydin<sup>4</sup>

## Abstract

We propose a novel method for gradient-based optimization of black-box simulators using differentiable local surrogate models. In fields such as physics and engineering, many processes are modeled with non-differentiable simulators with intractable likelihoods. Optimization of these forward models is particularly challenging, especially when the simulator is stochastic. To address such cases, we introduce the use of deep generative models to iteratively approximate the simulator in local neighborhoods of the parameter space. We demonstrate that these local surrogates can be used to approximate the gradient of the simulator, and thus enable gradient-based optimization of simulator parameters. In cases where the dependence of the simulator on the parameter space is constrained to a low dimensional submanifold, we observe that our method attains minima faster than all baseline methods, including Bayesian optimization, numerical optimization, and REINFORCE driven approaches.

## 1. Introduction

Simulator optimization aims to determine the parameters that lead to the “best” performance of a simulated system or device as defined through an objective function and potentially a set of constraints. Thus a typical simulator optimization problem is defined as

$$\arg \min_{\psi} f(\psi), \text{ such that } h(\psi) = 0, g(\psi) \leq 0,$$

where  $f$  is an objective with parameters  $\psi \in \mathbb{R}^n$ , and  $h$  and  $g$  are equality and inequality constraints respectively. In some domains, this is referred to as design optimization.

<sup>\*</sup>Equal contribution <sup>1</sup>Department of Physics, Imperial College London, United Kingdom <sup>2</sup>Department of Computer Science, National Research University Higher School of Economics, Russia <sup>3</sup>SLAC National Accelerator Laboratory, Menlo Park, CA, United States <sup>4</sup>Department of Engineering Science, University of Oxford, United Kingdom. Correspondence to: Sergey Shirobokov <s.shirobokov17@imperial.ac.uk>, Vladislav Belavin <vbelavin@hse.ru>.

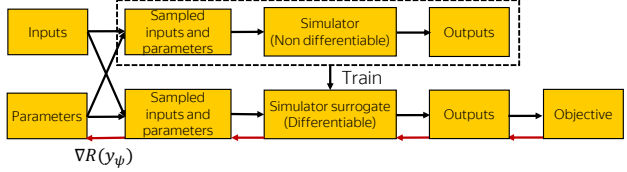


Figure 1. Surrogate optimization. Black: forward propagation, red: backpropagation. For further details refer to Algorithm 1.

In this work, we focus on a stochastic unconstrained variant of the above formulation wherein the objective function is expressed as an expected value of a cost or objective function  $f(\psi) = \mathbb{E}_{p(\mathbf{y};\psi)}[\mathcal{R}(\mathbf{y})]$ . The objective function  $\mathcal{R}$  is a function of the random variables  $\mathbf{y} \sim p(\mathbf{y}; \psi)$  with a density that is parameterized by the simulator parameters  $\psi$ . We also focus on the setting in which the cost of running the simulator is high, and thus aim to minimize the number of simulator calls needed for optimization. Such stochastic simulator optimization occurs in an array of scientific and engineering domains, especially in cases of simulation-based optimization relying on Monte Carlo techniques.

Several methods exist for such optimization, depending on the availability of gradients for the objective function (for a recent review see (Lei et al., 2017)). While gradient-based optimization has been demonstrated to work well for differentiable objective functions (Hu et al., 2019; Chang et al., 2016; de Avila Belbute-Peres et al., 2018; Degraeve et al., 2017), non-differentiable objective functions occur frequently in practice, e.g., where one aims to optimize the parameters of a system characterized by a Monte Carlo simulator that may only produce data samples from an intractable likelihood (Cranmer et al., 2019). In such cases, genetic algorithms (Bhaskar, 2001; Banzhaf et al., 1998), Bayesian optimization (Rasmussen, 2006), or numerical differentiation (Svanberg, 1987) are frequently employed. More recently, stochastic gradient estimators such as the REINFORCE algorithm (Williams, 1992) have been employed to estimate the gradient of non-differentiable functions (Stulp & Sigaud, 2013; Chen et al., 2016) and subsequently perform gradient descent based optimization.

In order to utilize the strengths of gradient-based optimization while avoiding the high variance often observed with stochastic gradient estimators like REINFORCE, our ap-

proach employs deep generative models as differentiable surrogate models to approximate non-differentiable simulators (Figure 1). Using these surrogates, we show that we can both approximate the stochastic behavior of the simulator and enable the direct gradient-based optimization of an objective function by parameterizing the surrogate model with the relevant parameters of the simulator. In high dimensional parameter spaces, training such surrogates over the complete parameter space becomes computationally expensive. Our technique, which we name local generative surrogate optimization (L-GSO), addresses this by using successive local neighborhoods of the parameter space to train surrogates at each step of parameter optimization. Our method works especially well when the parameters, which are seemingly high dimensional, live on a lower dimensional submanifold, as seen in practice in a variety of settings (Hoos & Leyton-Brown, 2014).

L-GSO relies primarily on two assumptions: (a) that the objective function is continuous and differentiable, and (b) that the parameters  $\psi$  are continuous variables. The first assumption may be relaxed by incorporating the objective into the surrogate. The second assumption may be relaxed in the case of discrete random variables by using discrete relaxation methods (Balog et al., 2017; Maddison et al., 2017), although this may inject bias into the surrogate.

In Section 2 we describe the local generative surrogate optimization algorithm. We cover related work in Section 3. In Section 4 we evaluate L-GSO on a set of toy problems and compare it with frequently used baseline methods including numerical differentiation, Bayesian optimization, and REINFORCE-based approaches. We also present results of a realistic use case in the high-energy physics domain. Section 5 presents our conclusions.

## 2. Method

### 2.1. Problem Statement

We target an optimization formulation applicable in domains where a simulator characterized by parameters  $\psi$  takes stochastic inputs  $\mathbf{x} \sim q(\mathbf{x})$  and produces outputs (observations)  $\mathbf{y} \sim p(\mathbf{y}|\mathbf{x}; \psi)$ . For example in the case of designing the shape of an experimental device,  $\mathbf{x}$  may represent random inputs to an experimental apparatus,  $\psi$  defines the shape of the apparatus, and  $p(\mathbf{y}|\mathbf{x}; \psi)$  encodes the impact of the apparatus on the input to produce observations  $\mathbf{y}$ . A task-specific objective function  $\mathcal{R}(\mathbf{y})$  encodes the quality of observations and may be optimized over the parameters  $\psi$  of the observed distribution as

$$\begin{aligned} \psi^* &= \arg \min_{\psi} \mathbb{E}[\mathcal{R}(\mathbf{y})] \\ &= \arg \min_{\psi} \int \mathcal{R}(\mathbf{y}) p(\mathbf{y}|\mathbf{x}; \psi) q(\mathbf{x}) d\mathbf{x} d\mathbf{y} . \end{aligned} \quad (1)$$

In cases when a simulator  $F$  can only draw samples from the distributions  $p(\mathbf{y}|\mathbf{x}; \psi)$  the optimization problem can be approximated as

$$\hat{\psi}^* = \arg \min_{\psi} \frac{1}{N} \sum_{i=1}^N \mathcal{R}(F(\mathbf{x}_i; \psi)) , \quad (2)$$

where  $\mathbf{y}_i = F(\mathbf{x}_i; \psi) \sim p(\mathbf{y}|\mathbf{x}; \psi)$ ,  $\mathbf{x}_i \sim q(\mathbf{x})$  and a Monte Carlo approximation to the expected value of the objective function is computed using samples drawn from the simulator. Note that  $F$  represents a stochastic process, which may itself depend on latent random variables.

### 2.2. Deep Generative Models as Differentiable Surrogates

Given a non-differentiable simulator  $F$ , direct gradient-based optimization of Eq. 1 is not possible unless one uses typically high variance stochastic gradient estimators such as REINFORCE. Instead, we propose to approximate  $F$  with a learned differentiable surrogate model  $\bar{\mathbf{y}} = S_{\theta}(\mathbf{z}, \mathbf{x}; \psi)$  that approximates  $F(\mathbf{x}; \psi)$ , where  $\mathbf{z} \sim p(\mathbf{z})$  is a latent variable accounting for the stochastic variation of the distribution  $p(\mathbf{y}|\mathbf{x}; \psi)$ . When the samples  $\bar{\mathbf{y}}$  are differentiable with respect to  $\psi$ , direct optimization of Eq. 1 becomes possible using the surrogate gradient estimator:

$$\nabla_{\psi} \mathbb{E}[\mathcal{R}(\mathbf{y})] \approx \frac{1}{N} \sum_{i=1}^N \nabla_{\psi} \mathcal{R}(S_{\theta}(\mathbf{z}_i, \mathbf{x}_i; \psi)) . \quad (3)$$

To obtain a differentiable surrogate capable of modeling a stochastic process,  $S$  is learned with a deep generative model. Such generative model learning can be done independently of the simulator optimization in Eq. 2 as it only requires samples from the simulator to learn the simulated stochastic process. Once learned, the generative surrogate can produce differentiable samples that are used to approximate the integration for the expected value of the objective function. Several types of generative models could be used, including generative adversarial networks (GANs) (Goodfellow et al., 2014), variational autoencoders (Kingma & Welling, 2013; Rezende et al., 2014), or flow based models (Rezende & Mohamed, 2015). In this paper we present results obtained using conditional variants of two recently proposed generative models, Cramer GAN (Bellemare et al., 2017) and the FFJORD continuous flow model (Grathwohl et al., 2018a), to show the independence of L-GSO from the choice of generative model.

### 2.3. Local Generative Surrogates

The L-GSO optimization algorithm is summarized in Algorithm 1. Using a sample of values for  $\psi$  and input samples

of  $\mathbf{x}$ , a set of training samples for the surrogate are created from the simulator  $F$ . The surrogate training step 8 refers to the standard training procedures for the chosen generative model (additional details about model architectures and training hyperparameters are given in Appendix A). The learned surrogate is used to estimate the gradient of the objective function with backpropagation through the computed expectation of Eq. 3 with respect to  $\psi$ . Subsequently  $\psi$  is updated with a gradient descent procedure which we denote as *SGD* (stochastic gradient descent) in the algorithm. Due to the use of SGD, an inherently noisy optimization algorithm, the surrogate does not need to be trained until convergence but only sufficiently well to provide gradients correlated with the true gradient that produce useful SGD updates. The level of correlation of the gradients will control the speed of convergence of the method.

For high-dimensional  $\psi$ , a large number of parameter values  $\psi$  must be sampled to accurately train a single surrogate model to provide sufficiently well estimated gradients over the full parameter space that may be explored by gradient-based optimization. Thus optimization using a single upfront training of the surrogate model over all  $\psi$  becomes unfeasible. As such, we utilize a trust-region like approach (Sorensen, 1982) to train a surrogate model locally in the proximity of the current parameter value  $\psi$ . Thus we sample new  $\psi'$  around the current point  $\psi$  from the set  $U_\epsilon^\psi = \{\psi'; |\psi' - \psi| \leq \epsilon\}$ . Using this local model, a gradient at the current point  $\psi$  can be obtained and a step of SGD performed. After each SGD update of the parameters  $\psi$ , a new local surrogate is trained. As a result, we do not expect domain shift to impact L-GSO as it is retrained at each new parameter point.

In local optimization there are several hyperparameters that require tuning either prior to or dynamically during optimization. One must choose the sampling algorithm for  $\psi$  values in the region  $U_\epsilon^\psi$  in step 3 of Algorithm 1. In high-dimensional space, uniform sampling is inefficient, thus we have adopted the Latin Hypercubes algorithm (Iman et al., 1980).<sup>1</sup> One must also choose a proximity hyperparameter  $\epsilon$ , that controls the size of the region of  $\psi_i$  in which a set of  $\psi$  values is chosen to train a local surrogate.<sup>2</sup> This hyperparameter is similar to the step size used in numerical differentiation, affecting the speed of convergence as well as the overall behaviour of the optimization algorithm; if  $\epsilon$  is too large or too small the algorithm may diverge. In this paper we report experimental results with this hyperparameter tuned based on a grid search.

<sup>1</sup>A detailed study of alternative sampling techniques is left for future work.

<sup>2</sup>In the case of a deterministic simulator this parameter could be chosen proportionally to learning rate. However, if the objective function is stochastic, then one might want to choose  $\epsilon$  big enough so that  $\mathbb{E}[\mathcal{R}(\mathbf{y}_{\psi-\epsilon}) - \mathcal{R}(\mathbf{y}_{\psi+\epsilon})] > \text{Var}(\mathcal{R}(\mathbf{y}_\psi))$ .

---

**Algorithm 1** Local Generative Surrogate Optimization (L-GSO) procedure
 

---

**Require:** number  $N$  of  $\psi$ , number  $M$  of  $\mathbf{x}$  for surrogate training, number  $K$  of  $\mathbf{x}$  for  $\psi$  optimization step, trust region  $U_\epsilon$ , size of the neighborhood  $\epsilon$ , Euclidean distance  $d$

- 1: Choose initial parameter  $\psi$
  - 2: **while**  $\psi$  has not converged **do**
  - 3:   Sample  $\psi_i$  in the region  $U_\epsilon^\psi$ ,  $i = 1, \dots, N$
  - 4:   For each  $\psi_i$ , sample inputs  $\{\mathbf{x}_j^i\}_{j=1}^M \sim q(\mathbf{x})$
  - 5:   Sample  $M \times N$  training examples from simulator  $\mathbf{y}_{ij} = F(\mathbf{x}_j^i; \psi_i)$
  - 6:   Store  $\mathbf{y}_{ij}, \mathbf{x}_j^i, \psi_i$  in history  $H$   
 $i = 1, \dots, N; j = 1, \dots, M$
  - 7:   Extract all  $\mathbf{y}_l, \mathbf{x}_l, \psi_l$  from history  $H$ ,  
 iff  $d(\psi, \psi_l) < \epsilon$
  - 8:   Train generative surrogate model  
 $S_\theta(\mathbf{z}_l, \mathbf{x}_l; \psi_l)$ , where  $\mathbf{z}_l \sim \mathcal{N}(0, 1)$
  - 9:   Fix weights of the surrogate model  $\theta$
  - 10:   Sample  $\bar{\mathbf{y}}_k = S_\theta(\mathbf{z}_k, \mathbf{x}_k; \psi)$ ,  $\mathbf{z}_k \sim \mathcal{N}(0, 1)$ ,  
 $\mathbf{x}_k \sim q(\mathbf{x})$ ,  $k = 1, \dots, K$
  - 11:    $\nabla_\psi \mathbb{E}[\mathcal{R}(\bar{\mathbf{y}})] \leftarrow \frac{1}{K} \sum_{k=1}^K \frac{\partial \mathcal{R}}{\partial \bar{\mathbf{y}}_k} \frac{\partial S_\theta(\mathbf{z}_k, \mathbf{x}_k; \psi)}{\partial \psi}$
  - 12:    $\psi \leftarrow \text{SGD}(\psi, \nabla_\psi \mathbb{E}[\mathcal{R}(\bar{\mathbf{y}})])$
  - 13: **end while**
- 

The number of  $\psi$  values sampled in the neighborhood is another key hyperparameter. We expect the optimal value to be highly correlated with the dimensionality and complexity of the problem. In our experiments, we examine the quality of gradient estimates as a function of the number of points used for training the local surrogate. We observe that it is sufficient to sample  $O(D)$  samples in the neighbourhood of  $\psi$ , where  $D$  is the full parameter space dimensionality of  $\psi$ . In this case, our approach is observed to be competitive with the numerical optimization and REINFORCE approaches, which similarly expect  $O(D)$  samples for performing a gradient step (Stulp & Sigaud, 2013; Svanberg, 1987). However, in cases where the components of  $\psi$  relevant for the optimization lie on a manifold of dimensionality lower than  $D$ , i.e., intrinsic dimensionality  $d$  is smaller than  $D$ , we observe that L-GSO requires less than  $D$  samples for producing a reasonable gradient step, thus leading to the faster convergence of L-GSO than other methods.

Previously sampled data points can also be stored in history and later reused in our local optimization procedure (Algorithm 1). This provides additional training points for the surrogate as the optimization progresses. This results in a better surrogate model and, consequently, better gradient estimation. The ability of L-GSO to reuse previous samples is a crucial point to reduce the overall number of calls

to the simulator. This procedure was observed to aid both FFJORD and GAN models to attain the minimum faster and to prevent the optimization from diverging once the minimum has been attained.

The benefit of our approach, in comparison with numerical gradient estimation, is that a deep generative surrogate can learn more complex approximations of the objective function than a linear approximation, which can be beneficial to obtain gradients for surfaces with high curvature. In addition, our method allows a reduction of the number of function calls by reusing previously sampled points. Utilizing generative neural networks as surrogates also provides potential benefits such as Hessian estimation, that may be used for second-order optimization algorithms and/or uncertainty estimation, and possible automatic determination of a low-dimensional parameter manifold.

### 3. Related Work

Our work lives at the intersection of simulator optimization and likelihood-free inference. In terms of simulator optimization, our approach can be compared to Bayesian optimization (BO) with Gaussian process based surrogates (Rasmussen, 2006) and numerical derivatives (Svanberg, 1987). In comparison with BO, our optimization approach makes use of gradients of the objective surface approximated using a surrogate, which can result in a faster and more robust convergence in multidimensional spaces with high curvature (see the Rosenbrock example in Figure 3c). Importantly, our approach does not require covariance matrix inversion which costs  $O(n^3)$  where  $n$  is a number of observations, thus making it impractical to compute in high dimensional spaces. To make BO scalable, authors often make structural assumptions on the function that may not hold generally. For example, references (Wang et al., 2013; Djolonga et al., 2013; Garnett et al., 2014; Zhang et al., 2019), assume a low-dimensional linear subspace that can be decomposed in subsets of dimensions. In addition, BO may require the construction of new kernels (Gorbach et al., 2017), such as (Oh et al., 2018) which proposes a cylindrical kernel that penalizes close to boundary points in the search space. Our approach does not make structural assumptions of the parameter manifold or assumptions on the locality of the optimum. While our approach does not require the design of a task-specific kernel, it does require the selection of a surrogate model structure.

In connection with likelihood-free inference, one aim is to estimate the parameters of a generative process with neither a defined nor tractable likelihood. A major theme of this work is posterior or likelihood density estimation (Papamakarios et al., 2018; Lueckmann et al., 2018; Greenberg et al., 2019). Our work is similar in its use of sequentially trained generative models for density estimation,

but unlike this work we focus on optimizing any user-defined function, and not specifically a likelihood or posterior, and the sequential training of generative models is used to enable gradient estimation rather than updating a posterior. Other recent examples of work that address this problem include (Louppe et al., 2017; Grathwohl et al., 2018b; Ruiz et al., 2019). While the first reference discusses non-differentiable simulators, it targets tuning simulator parameters to match a data sample and not the optimization of a user-defined objective function  $\mathcal{R}$ .

Non-differentiable function optimization using REINFORCE stochastic gradient estimators is explored in Grathwohl et al. (2018b); Ruiz et al. (2019). These approaches are applicable to our setting and we provide comparison in our experiment. Instead of employing the simulator within the computation of high variance REINFORCE gradients, our approach builds a surrogate simulator approximation to estimate gradients.

Deep generative models approaches to optimization problems have been explored in (Gupta & Zou, 2019; Brookes et al., 2019). These approaches focus on posterior inference of the parameters given observations, whereas we focus on direct gradient based objective optimization. In addition, these algorithms assume that it is not costly to sample from the simulator to perform posterior estimation, while sampling from the simulator is considered to be the most computationally expensive step to be minimized in our approach. In addition, (Gómez-Bombarelli et al., 2018) use generative models to learn a latent space where optimization is performed, rather than direct optimization over the parameter space of a surrogate forward model as in our approach.

The success of our optimization procedure on high dimensional spaces with low dimensional submanifolds is consistent with findings on the approximation quality of deep networks and how they adapt to the intrinsic dimension of the data (Suzuki & Nitanda, 2019; Nakada & Imaizumi, 2019; Schmidt-Hieber, 2019). These results provide bounds on approximation quality that reduce with small intrinsic dimension. Although these results are restricted to specific function classes, they are suggestive of the benefits of deep generative modeling over submanifolds that we empirically observe for optimization.

### 4. Experiments

We evaluate our methods on five toy experiments in terms of the attained optima and the speed of convergence. The speed of convergence is measured in the number of simulator calls, as it is assumed that this is the most time consuming operation during the optimization. The toy experiments were chosen to explore low and high dimensional



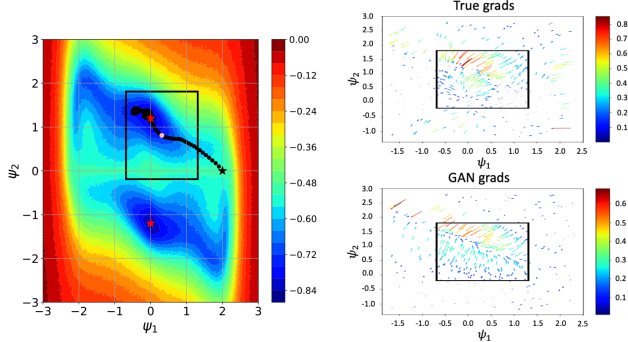


Figure 2. (Left) objective function surface of the "hump model" overlaid by the optimization path. Red stars represent the optimal values of the objective. (Right) True gradients and GAN gradients, calculated at the yellow point in the optimization path. Black rectangle correspond to the current  $\epsilon$  neighbourhood around yellow point. Full path animation is available at <https://doi.org/10.6084/m9.figshare.9944597.v3>.

optimization problems, as well as those with parameters on submanifolds. We also present results in a real physics experiment optimization.

#### 4.1. Toy Problems

**Three Hump Problem** In 2-dimensional probabilistic three hump problem we aim to find  $\psi$  that optimizes the following probabilistic process:

$$\begin{aligned} \psi^* &= \arg \min_{\psi} \mathbb{E}[\mathcal{R}(y)] = \mathbb{E}[\sigma(y - 10) - \sigma(y)], \text{ s.t.} \\ y &\sim \mathcal{N}(y; \mu_i, 1), i \in \{1, 2\} \\ \mu_i &\sim \mathcal{N}(x_i h(\psi), 1), \text{ P}(i = 1) = \frac{\psi_1}{\|\psi\|_2} = 1 - \text{P}(i = 2) \\ x_1 &\sim \mathcal{U}[-2, 0], \quad x_2 \sim \mathcal{U}[2, 5], \\ h(\psi) &= 2\psi_1^2 - 1.05\psi_1^4 + \psi_1^6/6 + \psi_1\psi_2 + \psi_2^2 \end{aligned} \quad (4)$$

**Rosenbrock Problem** In the N-dimensional Rosenbrock problem we aim to find  $\psi$  that optimizes the following probabilistic process:

$$\begin{aligned} \psi^* &= \arg \min_{\psi} \mathbb{E}[\mathcal{R}(y)] = \arg \min_{\psi} \mathbb{E}[y], \text{ s.t.} \\ y &\sim \mathcal{N}\left(y; \sum_{i=1}^{n-1} [(\psi_i - \psi_{i+1})^2 + (1 - \psi_i)^2] + x, 1\right), \\ x &\sim \mathcal{N}(x; \mu, 1), \quad \mu \sim \mathcal{U}[-10, 10] \end{aligned} \quad (5)$$

**Submanifold Rosenbrock Problem** To address problems where the parameters lie on a low dimension submanifold, we define the Submanifold Rosenbrock problem, with

a mixing matrix  $A$  to project the parameters onto a submanifold<sup>3</sup>. In our experiments  $\psi \in \mathbb{R}^{100}$  and  $A \in \mathbb{R}^{10 \times 100}$  has full row rank. Prior knowledge of  $A$  or the submanifold dimension is not used in the surrogate training. The optimization problem is thus defined as:

$$\begin{aligned} \psi^* &= \arg \min_{\psi} \mathbb{E}[\mathcal{R}(y)] = \arg \min_{\psi} \mathbb{E}[y], \text{ s.t.} \\ y &\sim \mathcal{N}\left(y; \sum_{i=1}^{n-1} [(\psi'_i - \psi'_{i+1})^2 + (1 - \psi'_i)^2] + x, 1\right), \\ \psi' &= A \cdot (\psi[\text{mask}]), \quad x \sim \mathcal{N}(x; \mu, 1), \quad \mu \sim \mathcal{U}[-10, 10] \end{aligned} \quad (6)$$

**Nonlinear Submanifold Hump Problem** This experiment explores non-linear submanifold embeddings of the parameters  $\psi$ . The embedding is through  $\hat{\psi} = B \tanh(A\psi)$ , where  $\psi \in \mathbb{R}^{40}$ ,  $A \in \mathbb{R}^{16 \times 40}$ ,  $B \in \mathbb{R}^{2 \times 16}$ , with  $A$  and  $B$  generated with the same procedure of in a previous problem.<sup>3</sup> The intrinsic dimension of the parameter space is equal to two in this example. The embedded parameters  $\hat{\psi}$  are then used in place of  $\psi$  in the three hump problem define in section 4.1. We use this example to additionally explore the number of parameter points needed per surrogate training for effective optimization on a submanifold.

**Neural Network Weights Optimization Problem** In this problem, we optimize neural network weights for regressing the Boston House Prices dataset (Harrison & Rubinfeld, 1978). As discussed by Li et al. (2018), neural networks are often overparameterized, thus having a smaller intrinsic dimensions than the full parameter space dimension. In this experiment we explore the optimization capability of L-GSO over the number of parameter space points needed per surrogate training, and, indirectly, measure bound on intrinsic dimensionality of the problem. The problem is defined as:

$$\begin{aligned} \psi^* &= \arg \min_{\psi} \mathbb{E}[\mathcal{R}(y)] = \arg \min_{\psi} \sqrt{\frac{1}{N} \sum_{i=1}^N (y - y_{\text{true}})^2}, \\ \text{where } y &= \text{NN}(\psi, x), \quad x \sim \{x_i\}_{i=1}^{506} \end{aligned} \quad (7)$$

**Baselines** We compare L-GSO to several baselines: Bayesian optimization using Gaussian processes with cylindrical kernels (Oh et al., 2018), which we denote "BOCK", numerical differentiation with gradient descent (referred to as numerical optimization), guided evolutionary strategies (Maheswaranathan et al., 2018), and the

<sup>3</sup>The orthogonal mixing matrix  $A$  is generated via a QR-decomposition of a random matrix sampled from the normal distribution.

REINFORCE-based “Learning To Simulate” method proposed in Ruiz et al. (2019), which we denote “LTS”, and the “Backpropagation through the Void” method by Grathwohl et al. (2018b), which we denote “Void”. The latter two baselines have recently been proposed for black-box optimization problems similar to ours. In cases where it is possible to compute true gradients of the objective function, we also present them as calculated by Pyro (Bingham et al., 2018).

Our primary metrics for comparison are the value of the objective function obtained from the optimization, and the number of simulator function calls needed to find a minimum. The latter metric assumes that the simulator calls are driving the computation time of the optimization. We tuned the hyper-parameters of all the baselines for their best performance.

**Results** As an illustrative example of L-GSO, we show the optimization path in  $\psi$  space for three hump problem in Figure 2. We also show gradient vector fields of the true model and of the GAN surrogate estimation at random  $\psi$  points during optimization, showing the successful non-linear approximation of the gradients by the surrogate. Visually, the true and the surrogate gradients closely match each other inside the surrogate training neighborhood (black rectangle). For an animated visualization of the optimization refer to the link in Figure 2.

For all experiments we rerun L-GSO on the same task five times with different random seeds. The variance is reported as bands in Figures 3 and 4.

The objective value as a function of the number of simulator calls for several experiments is presented in Figure 3. In all three experiments L-GSO outperforms REINFORCE based algorithms in speed of convergence by approximately an order of magnitude in number of simulator calls. Additionally, in all three experiments L-GSO attains the same optima as other converged methods and the speed of convergence is comparable to numerical optimization. In Figure 3a, Bayesian optimization converges faster than all other methods, which is not surprising in such as low dimensional problem. Conversely, in Figure 3b Bayesian optimization struggles to find the optimum due to the high curvature of the objective function, whereas the convergence speed of L-GSO is on par with numerical optimization. In general, L-GSO has several advantages over Bayesian optimization: (a) it is able to perform optimization without specification of the search space, i.e.,  $\psi \in \mathbb{R}^p$ , (b) the algorithm is embarrassingly parallelizable, though it should be noted that BO parallelization is an active area of research (Wang et al., 2016).

For completeness, in Table 1 we present difference between surrogate and true gradients (bias) as well as gra-

Table 1. Gradient difference (Left) and gradient variance (Right) for Rosenbrock problem.

Model	Gradient bias	Gradient variance
LTS [(Ruiz et al., 2019)]	$0.84 \pm 0.01$	$38 \pm 13$
Void model [(Grathwohl et al., 2018b)]	$1.21 \pm 0.02$	$319 \pm 51$
Numerical differentiation	$0.56 \pm 0.01$	$0.60 \pm 0.01$
L-GSO (FFJORD surrogate)	$0.98 \pm 0.03$	$0.001 \pm 0.001$
L-GSO (GAN surrogate)	$1.06 \pm 0.05$	$0.08 \pm 0.01$

dient variance for the Rosenbrock problem. The bias is calculated as:  $\text{GradDiff} = \left\| \frac{\nabla \psi_{\text{true}}}{\|\nabla \psi_{\text{true}}\|_2} - \frac{\nabla \psi_{\text{surr}}}{\|\nabla \psi_{\text{surr}}\|_2} \right\|_2$ , where  $\nabla \psi_{\text{true}}$  is a gradient from our toy simulator and  $\nabla \psi_{\text{surr}}$  is a gradient from the surrogate. We define the variance of the gradient as follows: for the current value of  $\psi$  during optimization, we run our surrogate  $n$  times and obtain gradients for  $\psi_1, \dots, \psi_n$ , and calculate the variance for each dimension in  $\psi$ . Thus we obtain a vector  $\text{Var}(\psi) = (\text{Var}(\psi^0), \dots, \text{Var}(\psi^p))$ . The norm of this vector is an estimator of gradient variance. We notice that the variance of the gradients of L-GSO is significantly smaller while the bias is comparable to that of REINFORCE based methods.

While L-GSO is comparable with baseline methods in the aforementioned experiments, we can observe the benefits of L-GSO in problems with parameter submanifolds, i.e. the Submanifold Rosenbrock, Nonlinear Submanifold Hump Problem and Neural Network Weights Optimization problems where the relevant  $\psi$  parameters live on a latent low-dimensional manifold. No prior knowledge of the submanifold is used in the training and we treat all the dimensions of  $\psi$  equally for all algorithms. The objective value as a function of the number of simulator calls can be seen in Figures 3c and 4 where we observe that L-GSO outperforms all baseline methods. We also observe that Bayesian Optimization was frequently not able to converge on such problems. Additionally, in all experiments, numerical optimization and/or BOCK outperform the REINFORCE-based approaches under consideration.

Figure 4 compares L-GSO implementations trained with differing numbers of parameter space points used per surrogate training. In the submanifold problems, L-GSO converges fastest with far fewer parameter points than the full dimension of the parameter space. This indicates that L-GSO is able to learn about the latent manifold of the data, rather than needing to fully sample the volume around a current parameter point. Leveraging the conditional generative network, the algorithm learns the correlations between different dimensions of  $\psi$  and is also able to inter-

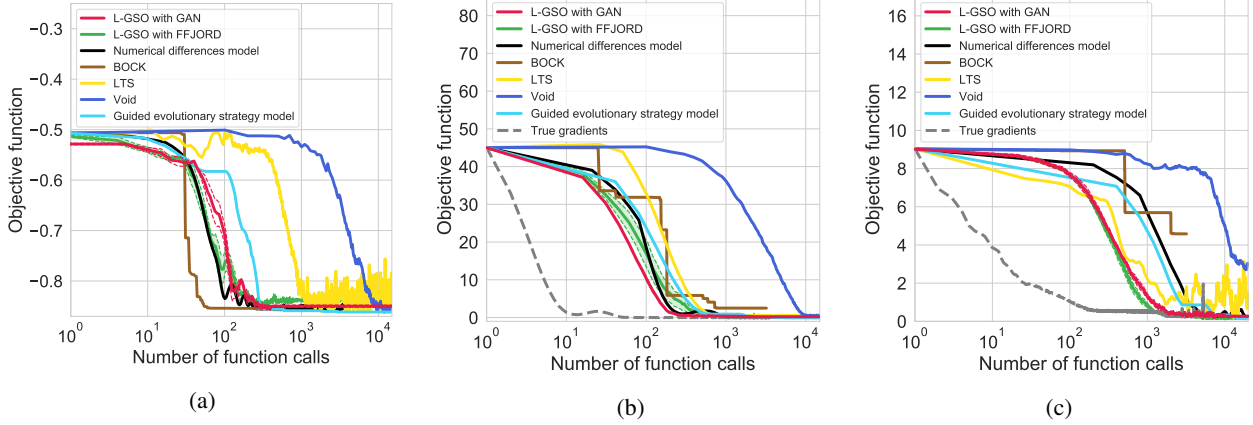


Figure 3. The objective function value on the toy problems for baselines and our method. (a) Three hump problem, (b) Rosenbrock problem (Rosenbrock, 1960) in 10 dimensions, initial point is  $\vec{z} \in \mathbb{R}^{10}$ . (c) Submanifold Rosenbrock Problem in 100 dimensions, initial point is  $\vec{z} \in \mathbb{R}^{100}$ . True gradients are shown in grey dashed curves when available. Shaded region corresponds to  $1\sigma$  confidence intervals.

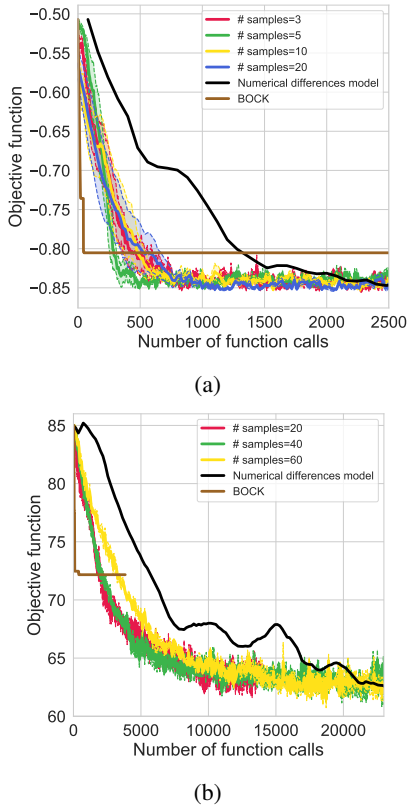


Figure 4. The objective function value on the toy problems for baselines and our method for different number of samples per epochs. (a) Nonlinear Submanifold Three Hump problem,  $\psi \in \mathbb{R}^{40}$ , (b) Neural Network Weights Optimization problem,  $\psi \in \mathbb{R}^{91}$ .

polate between different sampled points. This allows the algorithm to obtain useful gradients in  $\psi$ , while using far fewer samples than numerical differentiation.

#### 4.2. Physics Experiment Example

We apply the L-GSO algorithm to optimize the parameters of a apparatus in a physics experiment setting that utilizes the physics simulation software GEANT4 (Agostinelli et al., 2003) and FairRoot (Al-Turany et al., 2012). In this example, muon particles pass through a multi-stage steel magnet system, as seen in Figure 5. The muons are bent by the magnetic field and simultaneously experience stochastic scattering as they pass through the steel which causes random variations in their trajectories. The coordinates perpendicular to incoming direction (the z-axis in Figure 5) when muons leave the magnet volume are recorded if they pass through the sensitive area of a detection apparatus. As muons are unwanted in the experiment, the objective is to minimize number of muons recorded by the detection apparatus by varying the geometry of the magnet.

The problem can be defined as follows: the inputs  $x$  correspond to the physical properties of the incoming muons, namely the momentum (P), the azimuthal angle with respect to the incoming axis ( $\phi$ ), the polar angle with respect to the incoming axis ( $\theta$ ), the charge  $Q$ , and  $x$ - $y$ - $z$  coordinate  $C$ . The observed output  $y$  is the muon coordinates on the plane transverse to the incoming  $z$ -axis as measured by the detection apparatus. The parameter  $\psi \in \mathbb{R}^{42}$  represents the geometry of the magnet. The magnet is constructed from six trapezoidal shapes with gaps each of which is described by seven parameters, as presented in Figure 5. The objective function we employ to penalize muons hitting the

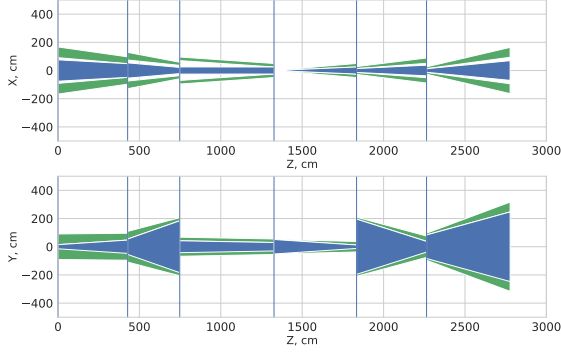


Figure 5. The  $x$ - $z$  axes and  $y$ - $z$  axes profiles of the magnet system being optimized (the post optimization shape is shown). Animation of optimization process is available at <https://doi.org/10.6084/m9.figshare.11778684.v1>.

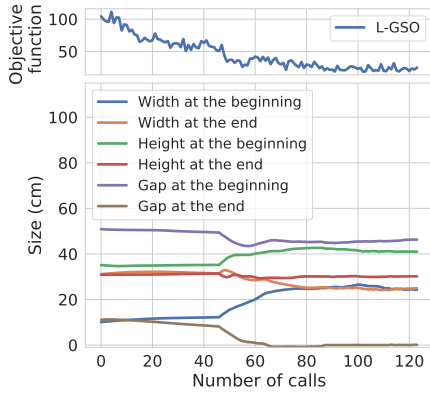


Figure 6. Optimization of the high energy physics example. (Top) objective function value during optimization. (Bottom)  $\psi$  Sub-sample of six parameters values during optimization.

detection apparatus is

$$\mathcal{R}(\mathbf{y}; \boldsymbol{\alpha}) = \sum_{i=1}^N \mathbb{1}_{Q_i=1} \sqrt{(\alpha_1 - (\mathbf{y}_i + \alpha_2))/\alpha_1} + \mathbb{1}_{Q_i=-1} \sqrt{(\alpha_1 + (\mathbf{y}_i - \alpha_2))/\alpha_1}, \quad (8)$$

where  $\mathbb{1}$  is the indicator function, and  $\alpha_1 = 5.6$  m and  $\alpha_2 = 3$  m define the detector sensitive region.

Results of the optimization using L-GSO with a Cramer GAN (Bellemare et al., 2017) as the deep surrogate are presented in Figure 6. L-GSO is successfully able to drive the objective function towards an optimum. A previous optimization of this magnet system was performed using Bayesian Optimization with Gaussian processes with RBF kernels (Baranov et al., 2017). The distributions of muons in the detection apparatus obtained by L-GSO is compared with BO optimization in Figure 7. The newly found optima has an objective function value approximately 25% smaller in comparison to the BO solution, while using ap-

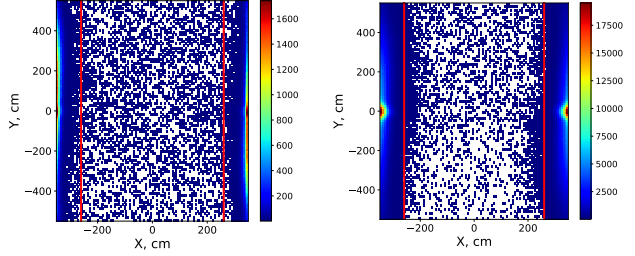


Figure 7. Muon hits distribution in the detection apparatus (depicted as red contour) obtained by Bayesian optimization (Left) and by L-GSO (Right), showing better distribution. Color represents number of the hits in a bin.

proximately the same budget of  $O(5,000)$  simulator calls. The L-GSO configuration is shorter and has lower mass than the BO solution, which can lead to both improved efficacy of the experiment and significant cost reduction.

## 5. Conclusions

We propose a novel approach for the optimization of stochastic non-differentiable simulators. Our proposed algorithm is based on deep generative surrogates, such as GANs or flow models, successively trained in local neighborhoods of parameter space during parameter optimization. We compare this against REINFORCE based baselines (Ruiz et al., 2019; Grathwohl et al., 2018b) as well as numerical differentiation and Bayesian optimization with Gaussian processes (Oh et al., 2018). Our method, L-GSO, is generally comparable to baselines in terms of speed of convergence, but is observed to excel in performance where simulator parameters lie on a latent low-dimensional submanifold of the whole parameter space. L-GSO is parallelizable, and has a range of advantages including low variance of gradient estimates, scalability to high dimensions, and applicability for optimization on high curvature objective function surfaces. We performed experiments on a range of toy problems and a real high-energy physics simulator. Our results improved on previous optimizations obtained with Bayesian optimization, thus showing the successful optimization of a complex stochastic system with a user-defined objective function.

For future work, it is of interest to investigate strategies of adaptive selection of the number of samples per iteration step as well as the size of the local sampling neighbourhood, and automatic determination of relevant parameter subspaces. It is also intriguing to explore performance and limitations of our approach from the perspective of higher-order optimization, since differentiable surrogates allow us to estimate derivatives of any order. Another interesting direction is to investigate the applications to uncertainty quantification over the obtained parameters.



## Acknowledgments

We would like to thank Gilles Louppe and Auralee Edele for their feedback, and Fedor Ratnikov for the fruitful discussions. MK is supported by the US Department of Energy (DOE) under grant DE-AC02-76SF00515 and by the SLAC Panofsky Fellowship. AU and VB are supported by Russian Science Foundation under grant agreement n° 19-71-30020. AGB is supported by EPSRC/MURI grant EP/N019474/1 and by Lawrence Berkeley National Lab.

## References

- Agostinelli, S. et al. GEANT4: A Simulation toolkit. *Nucl. Instrum. Meth.*, A506:250–303, 2003. doi: 10.1016/S0168-9002(03)01368-8.
- Al-Turany, M., Bertini, D., Karabowicz, R., Kresan, D., Malzacher, P., Stockmanns, T., and Uhlig, F. The fair-root framework. *Journal of Physics: Conference Series*, 396(2):022001, 2012. doi: 10.1088/1742-6596/396/2/022001.
- Balog, M., Tripuraneni, N., Ghahramani, Z., and Weller, A. Lost relatives of the gumbel trick. In *Proceedings of the 34th International Conference on Machine Learning-Volume 70*, pp. 371–379. JMLR. org, 2017.
- Banzhaf, W., Nordin, P., Keller, R., and Francone, F. *Genetic Programming: An Introduction*. Morgan Kaufmann Series in Arti. Elsevier Science, 1998. ISBN 9781558605107. URL <https://books.google.ch/books?id=1697qefFdtIC>.
- Baranov, A., Burnaev, E., Derkach, D., Filatov, A., Klyuchnikov, N., Lantwin, O., Ratnikov, F., Ustyuzhanin, A., and Zaitsev, A. Optimising the active muon shield for the SHiP experiment at CERN. *Journal of Physics: Conference Series*, 934: 012050, dec 2017. doi: 10.1088/1742-6596/934/1/012050. URL <https://doi.org/10.1088%2F1742-6596%2F934%2F1%2F012050>.
- Bellemare, M. G., Danihelka, I., Dabney, W., Mohamed, S., Lakshminarayanan, B., Hoyer, S., and Munos, R. The cramer distance as a solution to biased wasserstein gradients. *arXiv preprint arXiv:1705.10743*, 2017.
- Bhaskar, A. Principles of optimal design: Modeling and computation p. y. papalambros and d. j. wilde second edition. cambridge university press, the edinburgh building, cambridge cb2 2ru, uk. 2000. 390pp. illustrated. £27.95. isbn 0-521-62727-3. *The Aeronautical Journal* (1968), 105(1050):458–459, 2001. doi: 10.1017/S0001924000012458.
- Bingham, E., Chen, J. P., Jankowiak, M., Obermeyer, F., Pradhan, N., Karaletsos, T., Singh, R., Szerlip, P. A., Horsfall, P., and Goodman, N. D. Pyro: Deep universal probabilistic programming. *CoRR*, abs/1810.09538, 2018. URL <http://arxiv.org/abs/1810.09538>.
- Brookes, D. H., Park, H., and Listgarten, J. Conditioning by adaptive sampling for robust design. In *ICML*, 2019.
- Chang, M. B., Ullman, T., Torralba, A., and Tenenbaum, J. B. A compositional object-based approach to learning physical dynamics. *arXiv preprint arXiv:1612.00341*, 2016.
- Chen, Y., Hoffman, M. W., Colmenarejo, S. G., Denil, M., Lillicrap, T. P., and de Freitas, N. Learning to learn for global optimization of black box functions. *ArXiv*, abs/1611.03824, 2016.
- Cranmer, K., Brehmer, J., and Louppe, G. The frontier of simulation-based inference. *arXiv preprint arXiv:1911.01429*, 2019.
- de Avila Belbute-Peres, F., Smith, K. A., Allen, K. R., Tenenbaum, J. B., and Kolter, J. Z. End-to-end differentiable physics for learning and control. In *NeurIPS*, 2018.
- Degrave, J., Hermans, M., Dambre, J., and Wyffels, F. A differentiable physics engine for deep learning in robotics. In *Front. Neurobot.*, 2017.
- Djolonga, J., Krause, A., and Cevher, V. High-dimensional gaussian process bandits. In *Advances in Neural Information Processing Systems*, pp. 1025–1033, 2013.
- Garnett, R., Osborne, M. A., and Hennig, P. Active learning of linear embeddings for gaussian processes. In *Proceedings of the Thirtieth Conference on Uncertainty in Artificial Intelligence*, UAI’14, pp. 230–239, Arlington, Virginia, USA, 2014. AUAI Press. ISBN 9780974903910.
- Gómez-Bombarelli, R., Duvenaud, D., Hernández-Lobato, J. M., Aguilera-Iparraguirre, J., Hirzel, T. D., Adams, R. P., and Aspuru-Guzik, A. Automatic chemical design using a data-driven continuous representation of molecules. In *ACS central science*, 2018.
- Goodfellow, I. J., Pouget-Abadie, J., Mirza, M., Xu, B., Warde-Farley, D., Ozair, S., Courville, A., and Bengio, Y. Generative Adversarial Networks. *arXiv e-prints*, art. arXiv:1406.2661, Jun 2014.
- Gorbach, N., Bian, Y. A., Fischer, B., Bauer, S., and Buhmann, J. Model selection for gaussian process regression. pp. 306–318, 08 2017. ISBN 978-3-319-66708-9. doi: 10.1007/978-3-319-66709-6\_25.

- Grathwohl, W., Chen, R. T. Q., Bettencourt, J., Sutskever, I., and Duvenaud, D. FFJORD: free-form continuous dynamics for scalable reversible generative models. *CoRR*, abs/1810.01367, 2018a. URL <http://arxiv.org/abs/1810.01367>.
- Grathwohl, W., Choi, D., Wu, Y., Roeder, G., and Duvenaud, D. Backpropagation through the void: Optimizing control variates for black-box gradient estimation. In *International Conference on Learning Representations*, 2018b. URL <https://openreview.net/forum?id=SyzKdlbCW>.
- Greenberg, D. S., Nonnenmacher, M., and Macke, J. H. Automatic posterior transformation for likelihood-free inference. In *ICML*, 2019.
- Gupta, A. and Zou, J. Feedback gan for dna optimizes protein functions. *Nature Machine Intelligence*, 1:105–111, 2019.
- Harrison, D. and Rubinfeld, D. Hedonic housing prices and the demand for clean air. *Journal of Environmental Economics and Management*, 5:81–102, 03 1978. doi: 10.1016/0095-0696(78)90006-2.
- Hoos, H. and Leyton-Brown, K. An efficient approach for assessing hyperparameter importance. In *International conference on machine learning*, pp. 754–762, 2014.
- Hu, Y., Liu, J., Spielberg, A., Tenenbaum, J. B., Freeman, W. T., Wu, J., Rus, D., and Matusik, W. Chainqueen: A real-time differentiable physical simulator for soft robotics. In *2019 International Conference on Robotics and Automation (ICRA)*, pp. 6265–6271, May 2019. doi: 10.1109/ICRA.2019.8794333.
- Iman, R., Davenport, J., and Zeigler, D. *Latin hypercube sampling (program user’s guide). [LHC, in FORTRAN]*. 01 1980. ISBN SAND-79-1473 United StatesThu Feb 07 00:00:56 EST 2008Dep. NTIS, PC A05/MF A01.SNL; ERA-05-017293; EDB-80-043435English.
- Keskar, N. S. and Socher, R. Improving generalization performance by switching from adam to sgd. *ArXiv*, abs/1712.07628, 2017.
- Kingma, D. P. and Ba, J. Adam: A method for stochastic optimization, 2014.
- Kingma, D. P. and Welling, M. Auto-encoding variational bayes, 2013.
- Lei, G., Zhu, J., Guo, Y., Liu, C., and Ma, B. A review of design optimization methods for electrical machines. *Energies*, 10:1962, 11 2017. doi: 10.3390/en10121962.
- Li, C., Farkhoor, H., Liu, R., and Yosinski, J. Measuring the intrinsic dimension of objective landscapes. *ArXiv*, abs/1804.08838, 2018.
- Louppe, G., Hermans, J., and Cranmer, K. Adversarial variational optimization of non-differentiable simulators. *ArXiv*, abs/1707.07113, 2017.
- Lueckmann, J.-M., Bassetto, G., Karaletsos, T., and Macke, J. H. Likelihood-free inference with emulator networks. In *AABI*, 2018.
- Maddison, C., Mnih, A., and Teh, Y. The concrete distribution: A continuous relaxation of discrete random variables. 2017.
- Maheswaranathan, N., Metz, L., Tucker, G., Choi, D., and Sohl-Dickstein, J. Guided evolutionary strategies: augmenting random search with surrogate gradients. In *ICML*, 2018.
- Nakada, R. and Imaizumi, M. Adaptive approximation and estimation of deep neural network to intrinsic dimensionality. *ArXiv*, abs/1907.02177, 2019.
- Oh, C., Gavves, E., and Welling, M. Bock : Bayesian optimization with cylindrical kernels. In *ICML*, 2018.
- Papamakarios, G., Sterratt, D. C., and Murray, I. Sequential neural likelihood: Fast likelihood-free inference with autoregressive flows. *ArXiv*, abs/1805.07226, 2018.
- Rasmussen, C. E. Gaussian processes for machine learning. MIT Press, 2006.
- Rezende, D. J. and Mohamed, S. Variational inference with normalizing flows. *arXiv preprint arXiv:1505.05770*, 2015.
- Rezende, D. J., Mohamed, S., and Wierstra, D. Stochastic backpropagation and approximate inference in deep generative models. In *Proceedings of the 31st International Conference on International Conference on Machine Learning - Volume 32, ICML’14*, pp. II–1278–II–1286. JMLR.org, 2014.
- Rosenbrock, H. H. An Automatic Method for Finding the Greatest or Least Value of a Function. *The Computer Journal*, 3(3):175–184, 01 1960. ISSN 0010-4620. doi: 10.1093/comjnl/3.3.175. URL <https://doi.org/10.1093/comjnl/3.3.175>.
- Ruiz, N., Schuler, S., and Chandraker, M. Learning to simulate. In *International Conference on Learning Representations*, 2019. URL <https://openreview.net/forum?id=HJgkx2Aqt7>.
- Schmidt-Hieber, J. Deep relu network approximation of functions on a manifold. *ArXiv*, abs/1908.00695, 2019.

- Smith, S. L., Kindermans, P.-J., Ying, C., and Le, Q. V. Don't decay the learning rate, increase the batch size, 2017.
- Sorensen, D. C. Newton's method with a model trust region modification. *SIAM J. Numer. Anal.*, 19(2):409–426, 1982.
- Stulp, F. and Sigaud, O. Policy improvement : Between black-box optimization and episodic reinforcement learning. 2013.
- Suzuki, T. and Nitanda, A. Deep learning is adaptive to intrinsic dimensionality of model smoothness in anisotropic besov space. *ArXiv*, abs/1910.12799, 2019.
- Svanberg, K. The method of moving asymptotes—a new method for structural optimization. 1987.
- Wang, J., Clark, S. C., Liu, E., and Frazier, P. I. Parallel bayesian global optimization of expensive functions. 2016.
- Wang, Z., Zoghi, M., Hutter, F., Matheson, D., and De Freitas, N. Bayesian optimization in high dimensions via random embeddings. In *Twenty-Third International Joint Conference on Artificial Intelligence*, 2013.
- Williams, R. J. Simple statistical gradient-following algorithms for connectionist reinforcement learning. *Mach. Learn.*, 8(3-4):229–256, May 1992. ISSN 0885-6125. doi: 10.1007/BF00992696. URL <https://doi.org/10.1007/BF00992696>.
- Zhang, M., Li, H., and Su, S. W. High dimensional bayesian optimization via supervised dimension reduction. In *IJCAI*, 2019.

### A.1. GAN Implementation

## A.2. FFJORD Implementation

Original version of FFJORD does not have a support of conditional input. To address this issue we rewrote one of the base layers that were used in FFJORD library. We have added additional two-layers network with hidden dimensionality equal 8 that takes as an input conditional information and injects it in base layer output as an additive bias term.

During optimization we are constantly monitoring various statistics between samples from simulator and surrogate. The example of such statistics is presented in Fig 8. This is done to ensure that the surrogate learn a meaningful approximation of the simulator on each iteration of optimization and if this is not the case, the user can further tune the model.

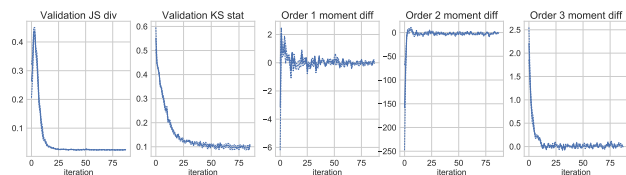


Figure 8. An example of monitored statistics during surrogate training for one iteration of optimization. Left to right: Jensen–Shannon divergence, Kolmogorov–Smirnov statistic, difference between order one, two and three moment of the distributions from simulator and surrogate.

## B. Optimization Implementation Details

Throughout all the experiments Adam (Kingma & Ba, 2014) optimizer with default hyperparameters and learning rate equal  $10^{-1}$  was used to perform update of the  $\psi$  parameters.

Latin Hypercube sampling window of size  $\epsilon = 0.2$  was used for the “Rosenbrock”, “Submanifold Rosenbrock”, “Nonlinear Submanifold Hump”, and “Neural Network Weights Optimization” problems,  $\epsilon = 0.5$  was used for “Three Hump” problem.

### B.1. Procedure For Mixing Matrix Generation

10-dimensional mixing matrix  $A$  could be generated with the following Python code:

[illegible]



## B.2. Procedure For Initialization of Neural Network For Boston Regression Problem

Neural network for Boston regression problem initialized as a two-layer network with tanh-nonlinearity with predefined weights, using PyTorch.

```
import torch
from torch import nn
def make_boston_net():
    torch.manual_seed(1337)
    net = nn.Sequential(
        nn.Linear(13, 6),
        nn.Tanh(),
        nn.Linear(6, 1)
    )
    initial_weights = torch.tensor(
        [0.0215, 0.0763, 0.0879, 0.0102,
         0.095, 0.0508, 0.088, 0.101,
         0.0782, 0.0684, 0.0658, 0.0509,
         0.0207, 0.0618, 0.0756, 0.00784,
         0.0968, 0.0685, 0.0113, 0.0745,
         0.00154, 0.0772, 0.0472, 0.000906,
         0.0723, 0.0779, 0.0594, 0.0785,
         0.0918, 0.0634, 0.0853, 0.105,
         0.00407, 0.0789, 0.0035, 0.0581,
         0.0375, 0.0632, 0.0669, 0.00293,
         0.0901, 0.0208, 0.0388, 0.0893,
         0.00104, 0.0598, 0.0745, 0.08,
         0.0283, 0.0106, 0.0371, 0.0667,
         0.0331, 0.0356, 0.0661, 0.0554,
         0.084, 0.0398, 0.00286, 0.0281,
         0.0246, 0.0208, 0.0358, 0.033,
         0.0421, 0.0505, 0.00544, 0.0269,
         0.00527, 0.0569, 0.00538, 0.0786,
         0.102, 0.0452, 0.0444, 0.105,
         0.0765, 0.0689, 0.0249, 0.0933,
         0.037, 0.0762, 0.0882, 0.0505,
         0.0688, 0.0666, 0.101, 0.0857,
         0.0488, 0.0303, 22.5328])
    net[0].weight.data = initial_weights[:
        6 * 13].view(6, 13).detach().clone()
    net[0].weight.data = net[0].weight.data.float()
    net[0].bias.data = initial_weights[6 *
        13: 6 * 13 + 6].view(6).detach().clone()
    net[0].bias.data = net[0].bias.data.float()

    net[2].weight.data = initial_weights[6
        * 13 + 6: 6 * 13 + 6 + 6].view(1,
        6).detach().clone().float()
    net[2].bias.data = initial_weights[6 *
        13 + 6 + 6: 6 * 13 + 6 + 6 + 1].view(1).detach().clone().float()
    net.requires_grad_(False)
    return net
```

## B.3. Numerical Derivatives

To obtain numerical derivatives of  $\mathcal{R}$  we are using central difference scheme:

$$f'_{\psi_i} \approx (\bar{\mathcal{R}}(\psi_1, \dots, \psi_i + \epsilon, \dots, \psi_p) - \bar{\mathcal{R}}(\psi_1, \dots, \psi_i - \epsilon, \dots, \psi_p)) / 2\epsilon, \quad (9)$$

Where,  $\bar{\mathcal{R}} = \frac{1}{N} \sum_{i=1}^N \mathcal{R}(F(z_i, x_i; \psi))$ ,  $x_i \sim p(\mathbf{X})$ ,  $z_i \sim p(\mathbf{Z})$ .

For all experiments we set  $\epsilon = 0.1$ . We can not use small  $\epsilon$  due to the stochastic nature of  $\bar{\mathcal{R}}$  (see appendix C, where we compare results with different values of  $\epsilon$ ).

## C. Grid Search of Optimal Parameters

### C.1. Grid Search Hyperparameters For L-GSO

We have optimized crucial hyperparameters of L-GSO, such as learning rate, size of the sampling neighbourhood  $\epsilon$  and the number of samples of  $\psi$  in this neighbourhood with grid search. The grid search for Three hump and Rosenbrock problem is presented in Figure 9a, 9b. As it can be seen, for both problems best quality is obtained when number of samples is approximately equal to the dimensionality of the problem and when learning rate is close to 0.1. We found that learning rate 0.1 is optimal for all the toy problems under consideration. Thus, we have fixed it to be 0.1 for other grid search experiments. In the Figure 10a, 10b we present the grid search for 100 dimensional Degenerate Rosenbrock problem for number of samples per iteration and size of the neighbourhood. We found that L-GSO is very sensitive to the size of the neighbourhood  $\epsilon$ , whereas surprisingly robust to the number of samples, as it is seen in Figure 10a.

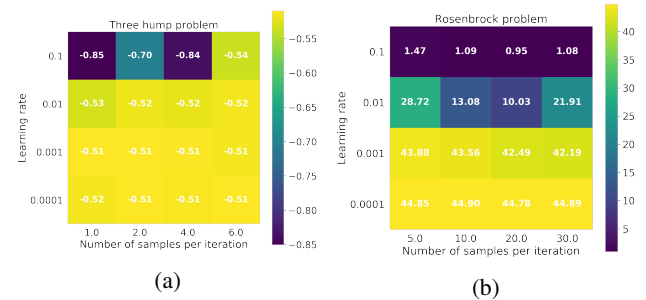


Figure 9. Grid search of learning rate and number of samples for L-GSO. Color represents final quality for Three hump problem (Left) and for Rosenbrock problem (Right).

### C.2. Grid Search Hyperparameters For Numerical Differentiation

We performed grid search over the order of numerical scheme  $n$  and step size  $h$  for numerical optimization for all four toy problems. As an example, the results for the

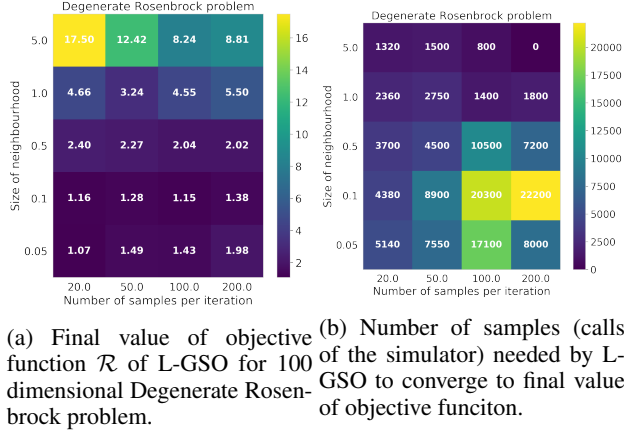


Figure 10.

toys problems are presented in Figure 11a, 11b, 12a, 12b, 13a, 13b,

## D. Details of the Physics Problem

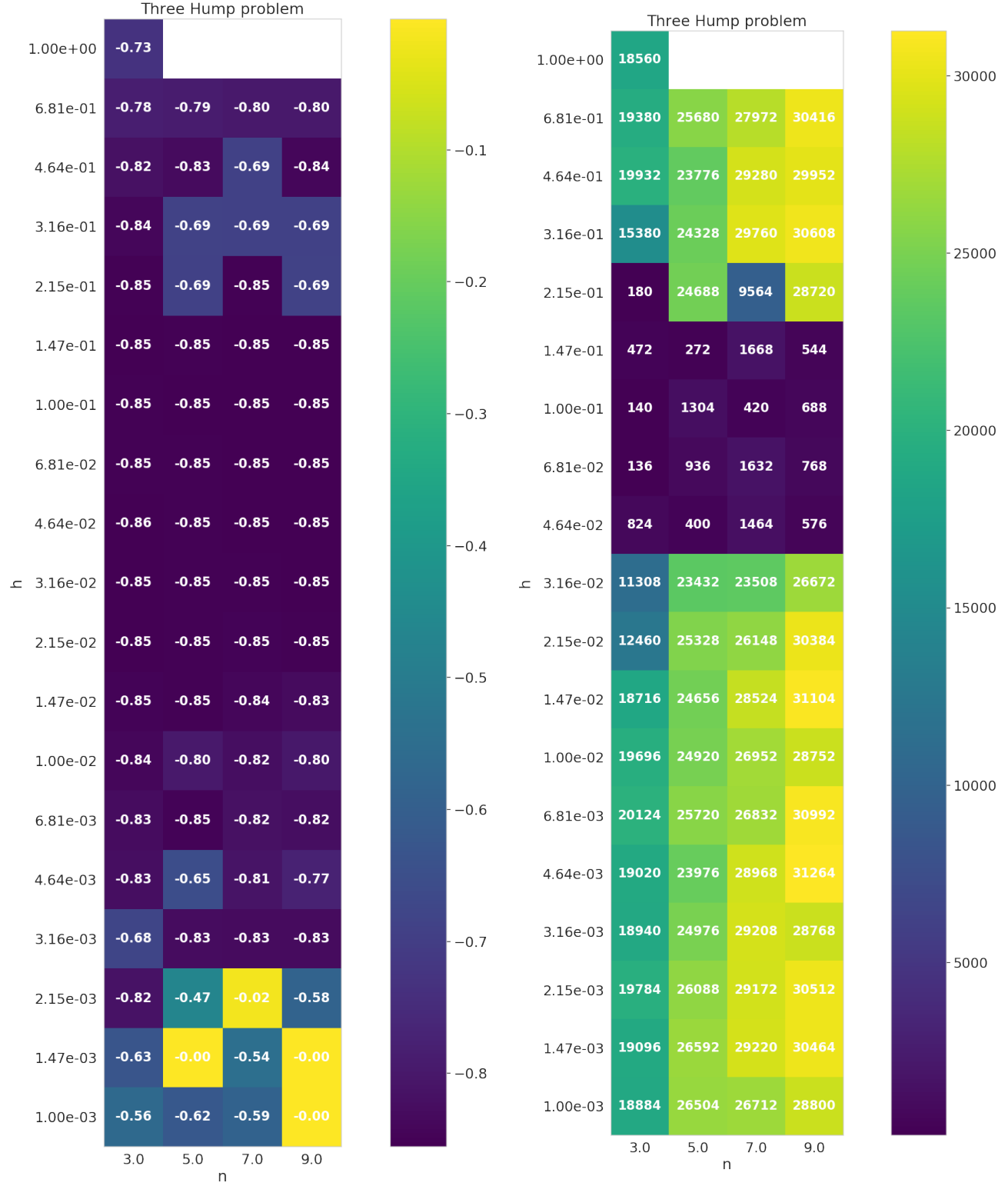
Mathematically, formulation is as follows:

$$X = \{P, \phi, \theta, Q, C\}, X \in \mathbb{R}^7, y \sim \mathbb{R}^2$$

where  $y$  is a simulator output representing hit coordinates in the sensitive detector.  $\psi \in \mathbb{R}^{42}$ .  $X$  is sampled from empirical distribution  $H$  (histogram), produced upfront. To make our optimization comparable with previously applied BO optimization, during optimization we have been working with subsample of  $H$  of size of order of  $O(500,000)$  events, same as in case of BO application. The objective function value reported in the Figure 6 is calculated on this sample. To perform cross-validation of the obtained optima, we run physics simulation on the largest available sample, which does not contain samples from  $H$ . We have also validated the BO optima on the same available sample. The comparison is presented in Table 2. Both BO and L-GSO have been compared on the simplified geometry of the experiment.

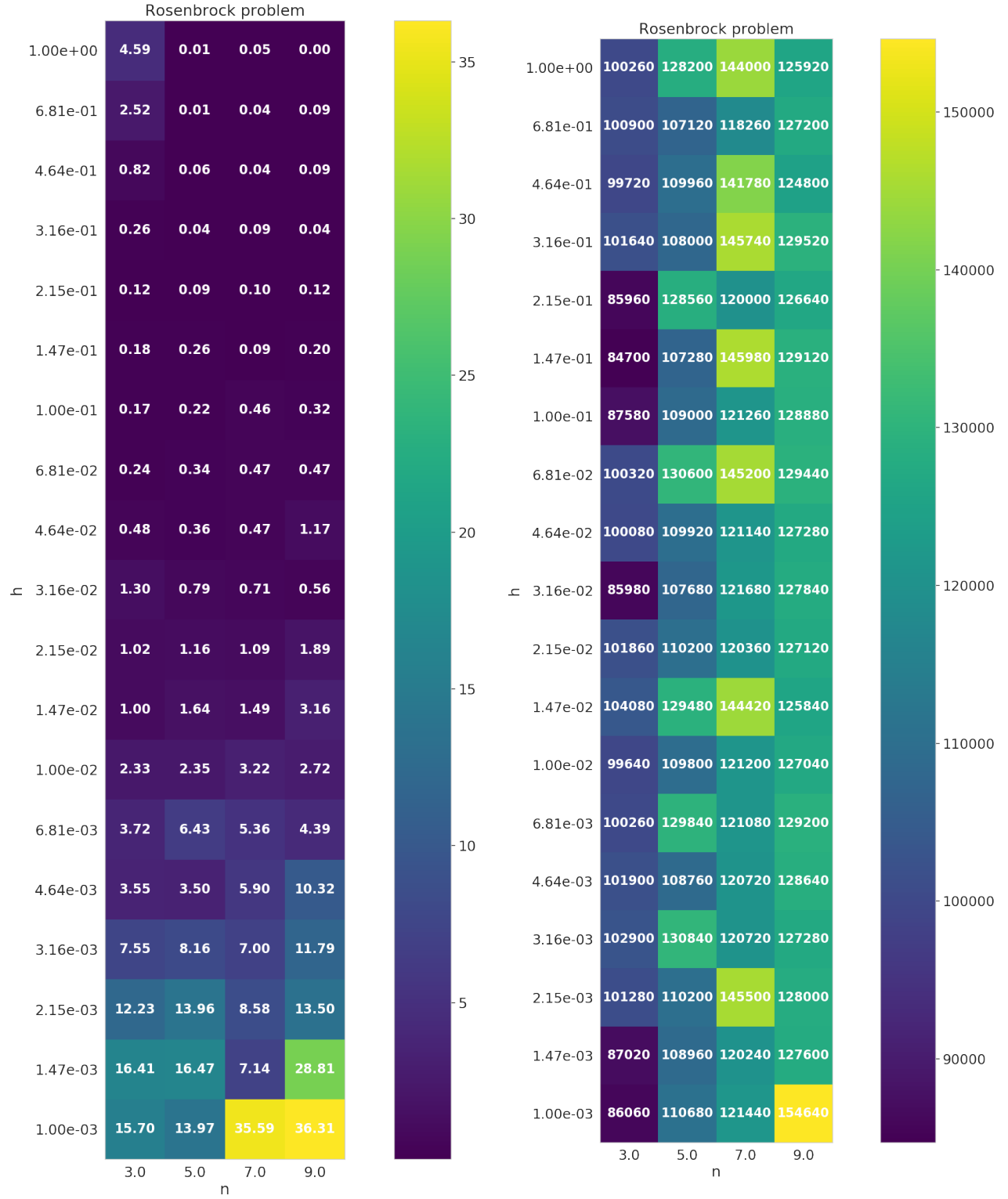
Table 2. Comparison of the optima, obtained by L-GSO and Bayesian optimization for the physics problem.

Algorithm	objective value	Magnet length (m)	Magnet weight (kt)
L-GSO	$\sim 2200$	33.39	1.05
BO	$\sim 3000$	35.44	1.27


 (a) Final value if objective function  $\mathcal{R}$  of numerical differentiation for hump problem.

(b) Number of samples(calls to the simulator) needed by numerical differences to converge.

Figure 11.

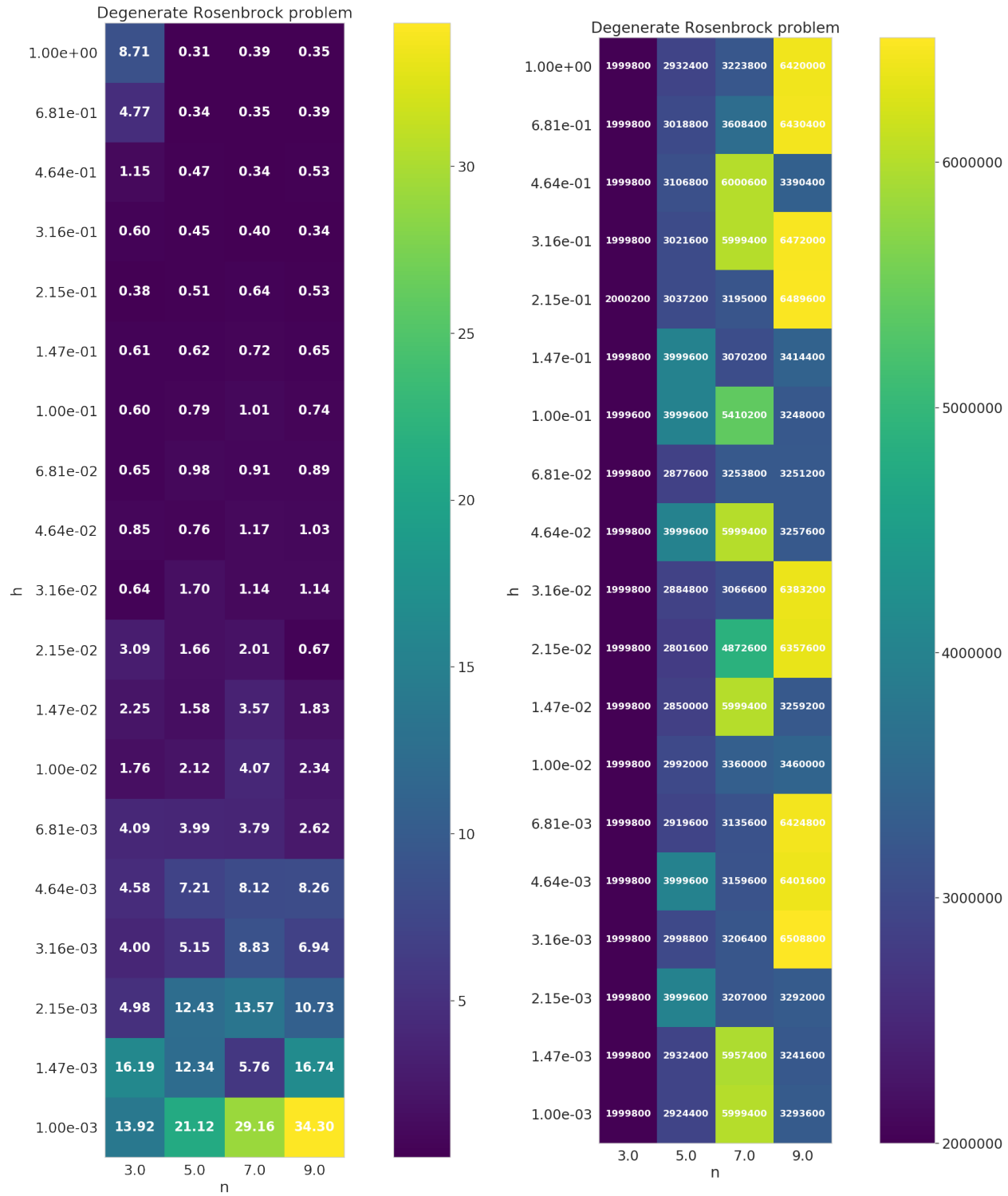


(a) Final value if objective function  $\mathcal{R}$  of numerical differentiation for 10-dim Rosenbrock problem.

(b) Number of samples(calls of the simulator) needed by numerical differentiation to converge.

Figure 12.




 (a) Final value of objective function  $\mathcal{R}$  of numerical differentiation for 100-dim Degenerate Rosenbrock problem.

(b) Number of samples(calls of the simulator) needed by numerical differentiation to converge.

Figure 13.